

# On The Inverse Relaxation Approach To Supercapacitors Characterization

Mikhail Evgenievich Kompan\* and Vladislav Gennadievich Malyshkin†

*Ioffe Institute, St. Petersburg, 194021*

(Dated: July 7, 2019)

**\$Id: inverserelaxation.tex,v 1.130 2020/08/13 10:38:21 mal Exp \$**

A novel inverse relaxation technique for supercapacitor characterization is developed, modeled numerically, and experimentally tested on a number of commercial supercapacitors. It consists in shorting a supercapacitor for a short time  $\tau$ , then switching to the open circuit regime and measuring an initial rebound and long-time relaxation. The results obtained are: the ratio of “easy” and “hard” to access capacitance and the dependence  $C(\tau)$ , that determines what the capacitance the system “feels” at time-scale  $\tau$ ; it can be viewed as an alternative to used by some manufacturers approach to characterize a supercapacitor by fixed capacitance and time-scale dependent internal resistance. Among the advantage of proposed technique is that it does not require a source of fixed current, what simplifies the setup and allows a high discharge current regime. The approach can be used as a replacement of low-frequency impedance measurements and can be effectively applied to characterization of supercapacitors and other relaxation type systems with porous internal structure. The technique can be completely automated by a microcontroller to measure, analyze, and output the results.

---

\* kompan@mail.ioffe.ru

† malyshki@ton.ioffe.ru

Dedicated to the memory of S.L. Kulakov

## I. INTRODUCTION

A distributed internal RC structure is manifested in electrical measurements of supercapacitors. The distribution is caused by hierarchical porous structure of electrodes. The two most commonly used technologies for manufacturing carbon structures for supercapacitor electrodes are Carbide-derived carbon (CDC) and Activated carbon. CDC materials are derived from carbide precursors[1]. An initial crystal structure of the carbide is the primary factor affecting CDC porosity. Activated carbon is typically derived from a charcoal or biochar[2]. It's structure is inherited from the starting material and has a surface area in excess of  $2,000\text{m}^2/\text{g}$  [3]. See [4] for a review of carbon materials used in supercapacitor electrodes. All the technologies used for supercapacitor manufacturing lead to a complex, “self-assembled” type of internal structure. In applications the most interesting is not the internal structure of a device per se, but it's manifestation in the electric properties.

While Li-ion systems are the most effective in energy storage applications[5], supercapacitors are the most effective in high-power applications. For Li-ion batteries the two characteristics are typically provided by manufacturers: specific energy and specific power. For supercapacitors the other two characteristics are typically provided by manufacturers: capacitance and internal resistance. Standard methods of characterization create a substantial uncertainty, because a supercapacitor's characteristics change during the discharge process. The knowledge about an internal *RC* distribution due to porous structure of the electrodes is missed from standard characterizations; it can be obtained from impedance type of measurements, but it is a low-current technique.

In this paper a novel technique of supercapacitor characterization is developed. The technique has all the measurements performed in time-domain, possibly at high current. The results obtained are the ratio of “easy” and “hard” to access capacitance and the dependence  $C(\tau)$ , that determines what the capacitance the system “feels” at time-scale  $\tau$  in at least three orders of  $\tau$  range. It can be effectively used as a replacement of low-frequency impedance measurements. The technique was microcontroller-automated to measure, analyze, and output the results.

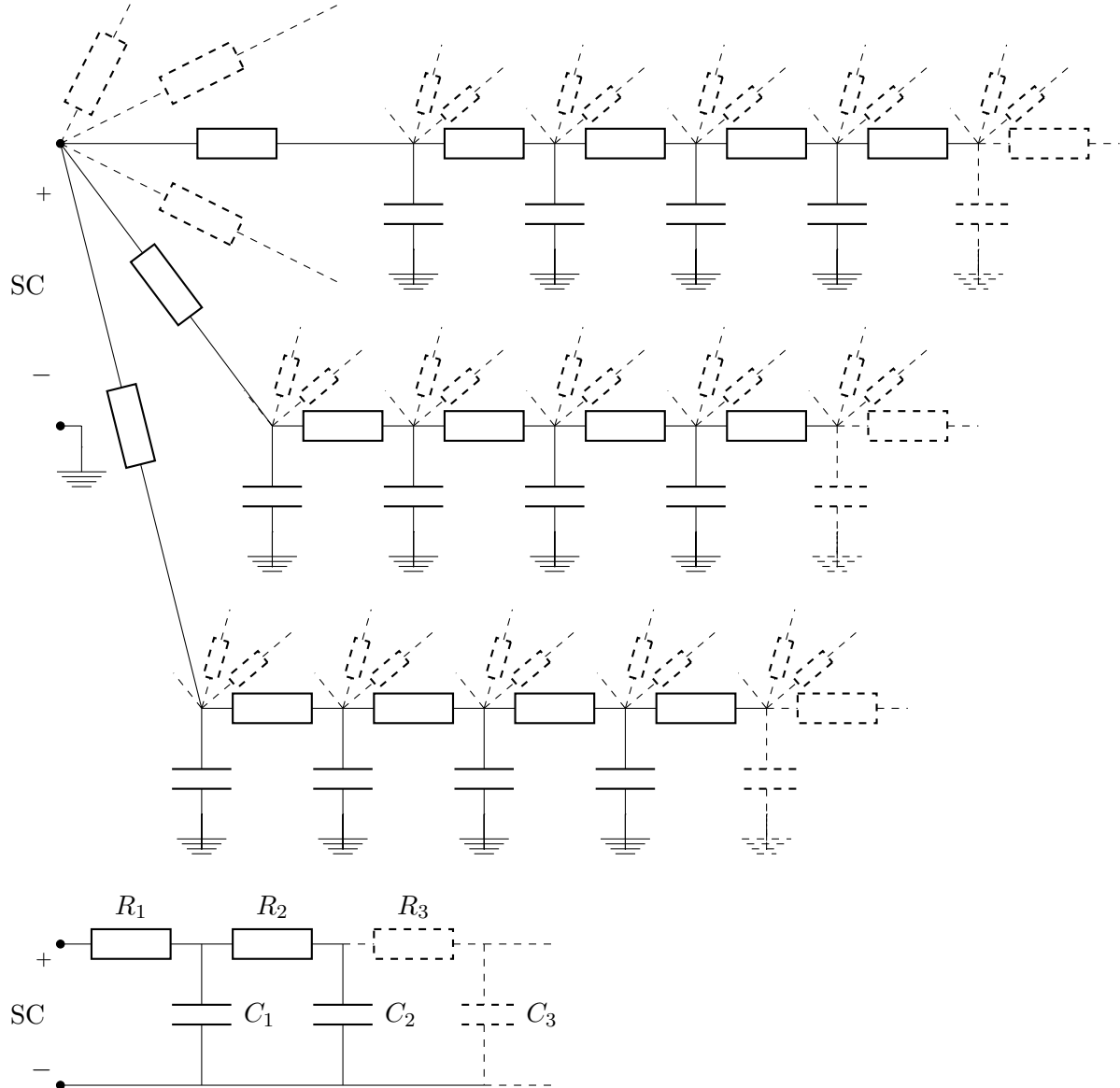


**FIG. 1:** Supercapacitor (SC) equivalent circuit corresponding to a hierarchical structure and the simplistic two- $RC$  model.

## II. INVERSE RELAXATION MODEL

Supercapacitors have multiple internal  $RC$ s, what corresponds to their hierarchical internal structure[4, 6–8]. The dynamics of such a system is rather complex, it is exhibited, for example, in multi-exponent evolution of  $U(t)$  relaxation (see experimental Fig. 8 below) and in deviation from a rectangle of a cyclic voltammetry (CV) plot. For an application in electronics the most convenient characteristic is: how a supercapacitor behaves at a given time-scale  $\tau$ . In terms

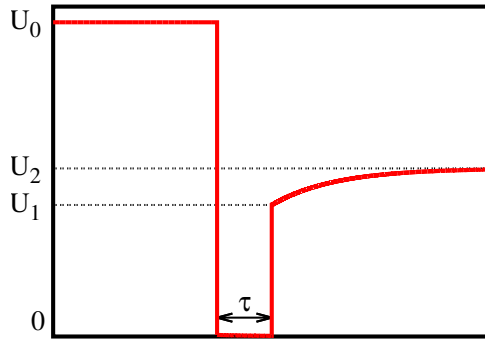


**FIG. 2:** A general form of  $U(t)$  dependence in inverse relaxation measurement technique. 1. Initial shorting for  $\tau \ll RC$ , the total charge passed is  $Q$ . 2. Immediate rise from  $U_s \approx 0$  to  $U_1$ . 3. In the open circuit regime a slow final rise from  $U_1$  to  $U_2$  due to internal charge redistribution.

of electric properties supercapacitor's electrodes internal porous structure can be considered as electric capacitance of two kind: “easy” (accessible at low  $\tau$ ) and “hard” (accessible only at high  $\tau$ ), Fig. 1. Actual distribution of the internal  $RC$  can be of different forms, and the internal structure manifests itself in the distribution of  $RC$ . This approach is more objective compared to impedance technique (which is a low amplitude technique), since it characterizes the discharge as a whole. When a supercapacitor is in the stationary state, all the capacitors in Fig. 1 model have equal potential, it is equal to the one on the electrodes, there is no internal current. When a supercapacitor is in a non-stationary state then internal charge redistribution takes place, it can be directly observed through the dynamics of electrodes potential.

Consider a measurement technique: the system is charged to some initial potential  $U_0$ , then it is short-circuited for a short interval time (lower than the supercapacitor's internal  $RC$ ) to create a non-stationary state, after that it is switched to the open circuit regime and  $U(t)$  is recorded to observe internal relaxation. The  $U(t)$  dependence is:

- First, from the initial potential  $U_0$  to almost zero (shorting to create a non-stationary state). Instead of shorting, a connection to a low-resistance circuit (we denote it  $R_s$ , a typical value is about  $10 - 50 m\Omega$ ) can be used (see Fig. 6 below), in this case the potential is non-zero, we denote the potential at the moment right before switching to the open circuit regime as  $U_s$ .

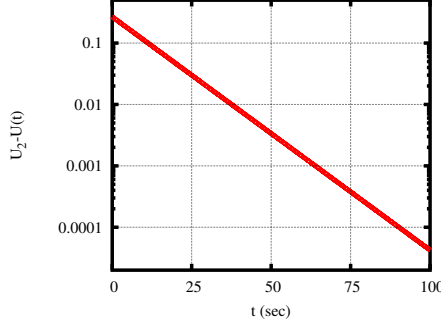
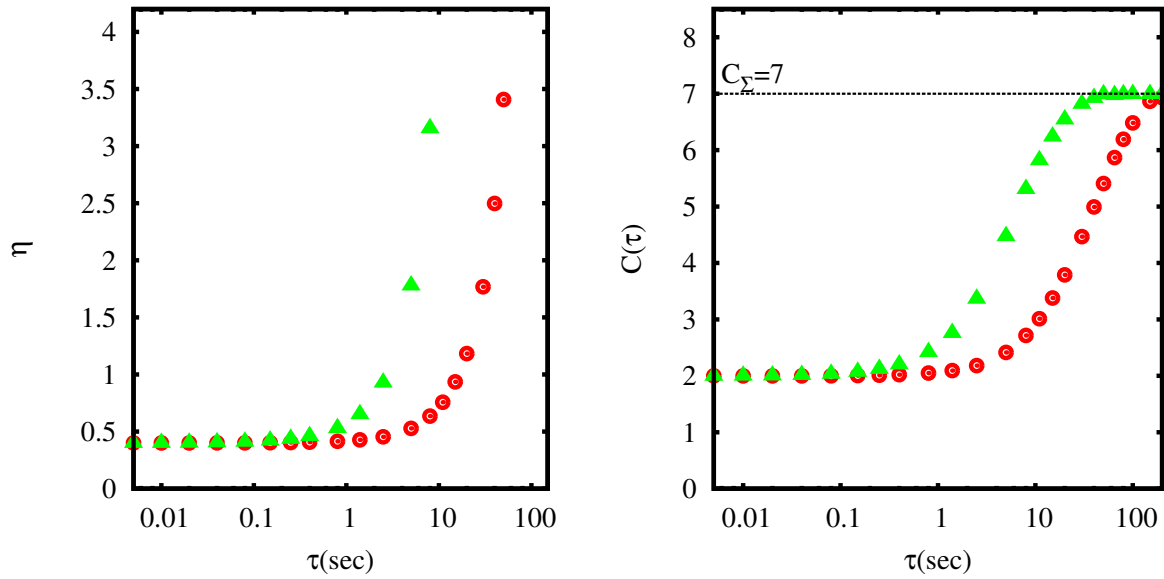


**FIG. 3:** A  $U_2 - U(t)$  evolution in two- $RC$  model systems.  $R_1 = 1\Omega$ ,  $C_1 = 2F$ ,  $R_2 = 8\Omega$ ,  $C_2 = 5F$ ). One can see a pure linear dependence ( $U_2 - U(t)$  is in log scale) for two- $RC$  model (single exponent).

- Then, after switching to the open circuit regime, the potential jumps from  $U_s$  to  $U_1$ . There is a similar current-interruption technique used in fuel cell measurements [9], page 64, the immediate rise voltage  $V = IR_i$  is an equivalent of  $U_1 - U_s$ .
- A slow final rise from  $U_1$  to  $U_2$ , Fig. 2. The  $U(t)$  relaxation from  $U_1$  to  $U_2$  may be of a single or multiple exponent type, this depends on the supercapacitor's internal structure. For two- $RC$  model a pure linear dependence is observed, single exponent relaxation in Fig. 3. For three- $RC$  supercapacitor model there are two exponents in  $U(t)$  evolution, one can clearly observe a deviation from the linear dependence in Fig. 5a below.
- While the  $U(t)$  measurement can be performed using traditional equipment a progress in microcontrollers (e.g. the STM32F103C8T6 ARM which costs below \$5 and has a 72Mhz CPU with 12-bit analog-to-digital converter (ADC)) allows the data to be easily recorded and stored. A microcontroller allows the total charge passed on the shorting stage to be calculated by direct integration:

$$Q = \int_0^\tau Idt \approx \sum_k \frac{U(t_k)}{R_s} (t_k - t_{k-1}) \quad (1)$$

Before we consider a more realistic model, let us demonstrate how the ratio of easy and hard to access capacitance can be found with the inverse relaxation technique for a *two- $RC$*  model. In this case the separation on “easy” and “hard” to access capacitance is trivial:  $C_1$



(a) The dependence of  $\eta$  on shorting time  $\tau$ . (b) The dependence  $C(\tau)$  on shorting time  $\tau$ .

**FIG. 4:** Two- $RC$  models:  $R_1 = 1\Omega$ ,  $C_1 = 2F$ ,  $R_2 = 8\Omega$ ,  $C_2 = 5F$  (circles) and  $R_1 = 1\Omega$ ,  $C_1 = 2F$ ,  $R_2 = 1\Omega$ ,  $C_2 = 5F$  (triangles). Both models have  $\eta(\tau = 0) = 0.4$ ,  $C(\tau = 0) = 2$ , and  $C(\tau = \infty) = 7$ .

is easy to access,  $C_2$  is hard to access. In two- $RC$  model an internal charge redistribution between  $C_1$  and  $C_2$  is:

$$\Delta Q_{C_1} = -\Delta Q_{C_2} \quad (2)$$

$$C_1 \cdot (U_2 - U_1) = C_2 \cdot (U_0 - U_2) \quad (3)$$

$$\eta = \frac{C_1}{C_2} = \frac{U_0 - U_2}{U_2 - U_1} \quad (4)$$

Important, that the ratio (4) of “easy” and “hard” capacitance does not depend on shorting time and on specific values of  $R_1$  and  $R_2$ . In two capacitors model the values  $U_0$ ,  $U_1$ , and  $U_2$  can be obtained analytically, but we are going to present a numerical solution with the goal to study a more complex model later on. In Fig. 4a the dependence of  $\eta$  on  $\tau$  is presented for two different two- $RC$  capacitor models with the same  $\eta$ . One can clearly see that the ratio (4) does not differ from the exact value  $C_1/C_2 = 0.4$  when shorting time  $\tau$  changes in two orders of magnitude range. A deviation from the constant arises only when shorting time  $\tau$  becomes comparable to the supercapacitor’s internal  $RC$ . For a small  $\tau$  charge redistribution inside a supercapacitor leads to  $\eta$  independence on  $\tau$  in a wide interval. When one starts to

increase the  $\tau$  — an initial charge redistribution becomes more prolonged and the deviation of  $\eta$  from a constant can be observed. The independence of  $\eta$  on  $\tau$  allows us to consider the ratio (4) as an immanent characteristic of the system. The  $\eta$  is obtained only from the measurement of the potential, and, while useful for structural characterization, lacks the information about absolute values. To obtain these the total charge  $Q$  is required, what requires a microcontroller to calculate (1). Once the  $Q$  is obtained, absolute values of  $R_1$  and  $C_1$  are:

$$C_1 \approx \frac{Q}{U_0 - U_1} \quad (5)$$

$$R_1 = \left[ \frac{U_1}{U_s} - 1 \right] R_s \quad (6)$$

The (5) follows from  $\tau \ll RC$ ; the (6) follows immediately from current balance:  $U_s/R_s = [U_1 - U_s]/R_1$ . Now consider an increase of  $\tau$  to the values above  $RC$ . Then  $R_1$  (6) stays the same, it does not depend on  $\tau$  at all. The  $C_1$  (5) increases with  $\tau$ , in the limit of large  $\tau$  it becomes equal to total capacitance  $C_\Sigma = C_1 + C_2 + \dots$ . Introduce

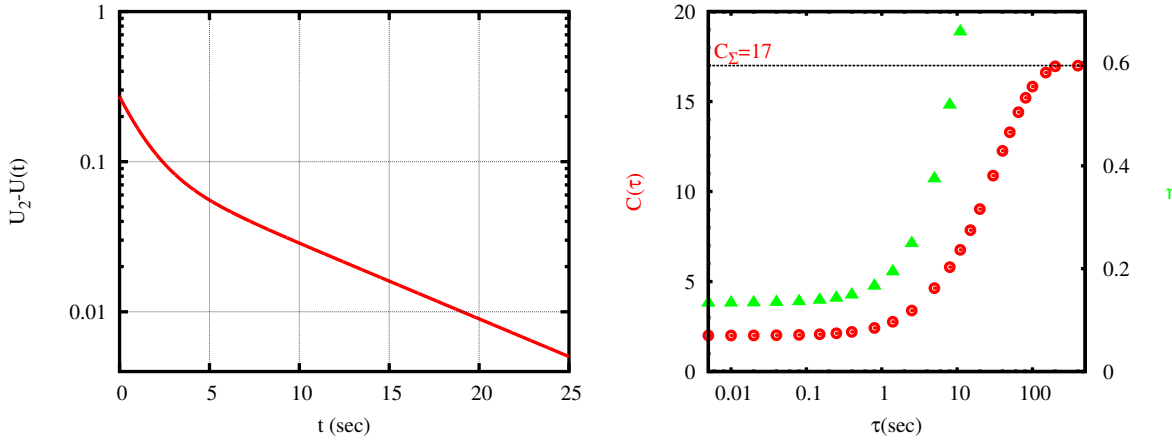
$$C(\tau) = \frac{Q(\tau)}{U_0 - U_1(\tau)} \quad (7)$$

that determines what the capacitance the system “feels” at time-scale  $\tau$ . In the Fig. 4b the dependence of  $C(\tau)$  is presented for two- $RC$  models. As expected  $C(\tau = 0) = C_1$  and  $C(\tau = \infty) = C_1 + C_2 + \dots$ .

The two-capacitors inverse relaxation model provides a single exponent behavior in  $U(t)$ . In a system with a number of porous branches the behavior is more complex. In the Fig. 5 a three- $RC$  supercapacitor model is presented. The system has multi-exponents in  $U(t)$  evolution, stable  $\eta$  for  $\tau \ll RC$  in two orders or magnitude range, and  $C(\tau)$  asymptotic  $C(\tau = 0) = C_1$  and  $C(\tau = \infty) = C_1 + C_2 + C_3 + \dots$ .

Regardless the specific model used for internal  $RC$  structure the simulation confirms that the  $\eta$  is stable for  $\tau$  varying in orders of magnitude range. This makes us to conclude that the ratio (4) is *more general*, than a specific model used. This ratio  $\eta$  is the system immanent property, it is the characteristic to separate easy- and hard- to access capacitance.

The characteristic  $C(\tau)$  shows what the capacitance “feels” at time-scale  $\tau$ . It can be measured from  $U(t)$  sampling with subsequent integration (1). An important advantage of  $C(\tau)$  is that it requires only  $\tau$ -long  $U(t)$  measurement: during shorting period and the potential immediately after switching to open circuit regime. The calculation of  $\eta$  requires



(a) A  $U_2 - U(t)$  evolution. A deviation from a linear dependence ( $U_2 - U(t)$  is in log scale) is clearly observed.

(b)  $C(\tau)$  (circles, left axis) and  $\eta$  (triangles, right axis).

**FIG. 5:** A three- $RC$  system:  $R_1 = 1\Omega$ ,  $C_1 = 2F$ ,  $R_2 = 1\Omega$ ,  $C_2 = 5F$ ,  $R_3 = 2\Omega$ ,  $C_3 = 10F$ .

the potential  $U_2$ , what may take much longer than  $\tau$  to measure, this makes  $\eta$  much more susceptible to charge leaks. The  $C(\tau)$  has a very clear practical meaning: If partial discharge takes time  $\tau$ , what is the ratio of charge/potential change for the  $\tau$ . This makes the inverse relaxation technique a well suitable tool for characterization of supercapacitors and other relaxation type systems with porous structure.

### III. THE EXPERIMENTAL MEASUREMENT OF SUPERCAPACITORS

The scheme in Fig. 6 provides an implementation of the inverse relaxation measurement technique. It consists of two computer-controlled switches “Charge” and “Short” (they can be either MOSFET transistors or fast mechanical relays); the output potential  $U(t)$  is measured by ADC port of a computer. If the controller has more than a single ADC, then it is convenient also to record the potential  $U^*(t)$  directly from  $R_s$ , this allows us to increase measurement precision and we can avoid (8) calibration of the  $R_s$ , which is required when a single potential  $U(t)$  is recorded: the resistance of “Short” switch is combined with the  $R_s$ .

Measured potentials, before connecting to ADC ports, must be passed through a operational amplifier with MOSFET input, e.g. AD823, to decrease parasitic discharge and, especially for two-potential measurement setup, we can set operational amplifier to a constant amplification

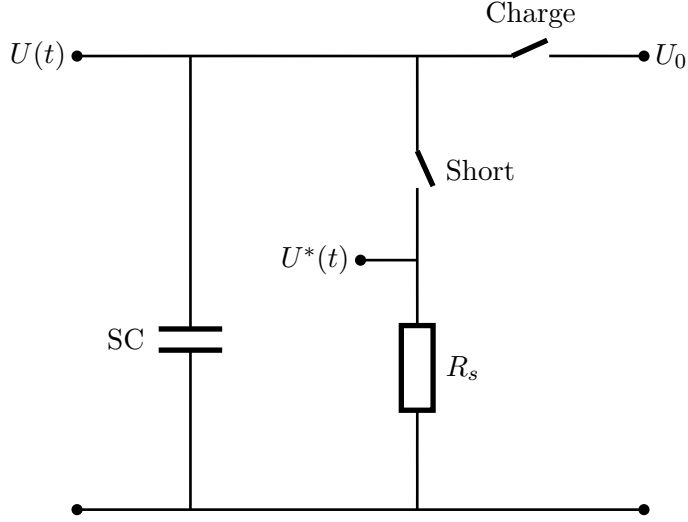


**FIG. 6:** Supercapacitor (SC) measurement circuit.

to bring small potential on shorting stage to the range of maximal ADC precision.

When working in a regime of single-potential recording the “on”-resistance of the “Short” switch is combined with the  $R_s$ . We can consider some “effective”  $R_s$  to enter (6) and the “Short” switch to be ideal. To obtain the value of an “effective”  $R_s$  correctly one can either:

- Do a calibration to total charge:

$$R_s \approx \frac{1}{CU_0} \int_0^\tau U(t) dt \quad \tau \gg RC \quad (8)$$

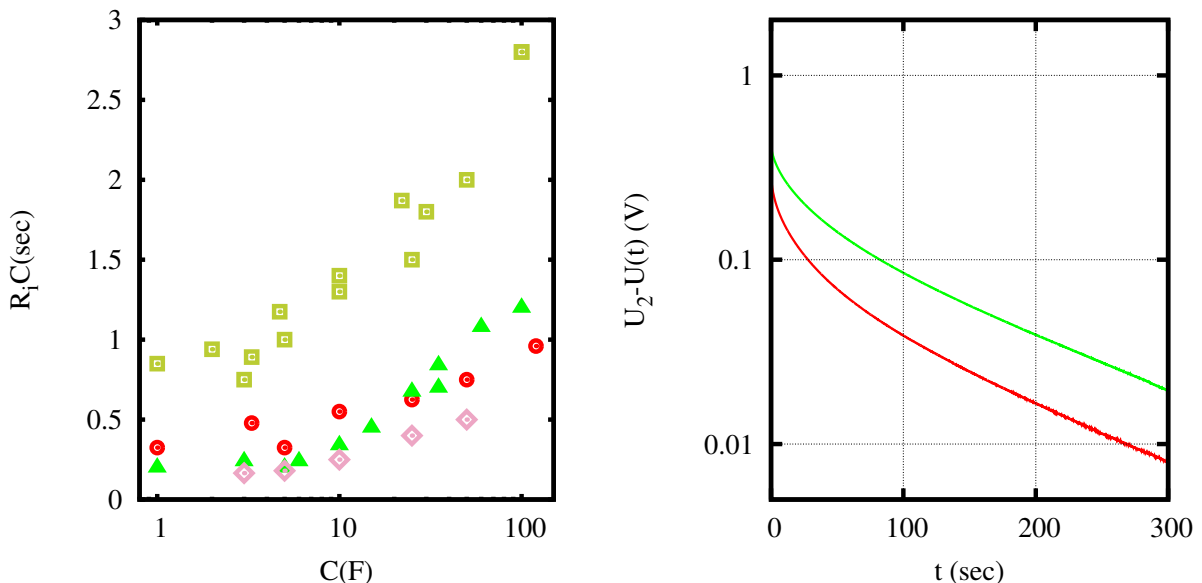
- Disconnect SC, put “Short” and “Charge” switches to “on” state, and connect the  $U_0$  terminal to a fixed current source, typically about a few ampere. Measured potential  $U$  determines the value of effective  $R_s$ , this is a variant of four-terminal sensing technique.

In the setup used by the authors an “effective”  $R_s$  was  $0.020\Omega$ .

We tested four commercial supercapacitors: AVX-SCCS20B505PRBLE, Eaton-HV1020-2R7505-R, IC-505DCN2R7Q, and Nesscap-ESHSR-0005C0-002R7; all 5F with 2.7V max. In Fig. 7 internal  $R_iC$  time is presented as a function of nominal capacitance for supercapacitors of the same series according to manufacturer datasheets. The  $R_iC$  depends mostly on the technology used and increases slowly with the capacitance. Supercapacitors have a developed internal structure, which manifests itself in multi-exponent  $U(t)$  dependence on inverse relaxation stage, see Fig. 8, which illustrates that inverse relaxation is typically **not** a single-exponent type of behavior. The relaxation at small time is faster than at large time. An

**FIG. 7:** The internal  $R_iC$  time as a function of capacitance according to datasheet for commercial supercapacitors of the manufacturers: AVX (circles), EATON (triangles), IC (squares), and Maxwell (rhombuses). The  $R_i$  is taken from the fields “ESR Max DC”, “Maximum initial ESR”, “DC ESR”, and “ESR DC Typical (10ms)” respectively.

**FIG. 8:** The  $U_2 - U(t)$  (in log scale) for AVX-SCCS20B505PRBLE (red) and Eaton-HV1020-2R7505-R (green). A deviation from a linear dependence is clearly observed. A “noise” observed at large  $t$  is due to exponentially small value of  $U_2 - U(t)$ , the situation can be improved by using a high quality ADC.



ultimate situation of such a behavior is presented in Fig. 5a for a model system. The deviation  $\log(U_2 - U(t))$  from a linear law is related to a distributed internal  $RC$ . Fitting of a multi-exponent  $U(t)$  relaxation is a common field of study[8]. A deviation from a single exponent (linear dependence in log axis) can be used as a source of information about supercapacitor’s internal structure. However, such an approach is more susceptible to measurement errors<sup>1</sup> and has interpretation difficulty.

Let us start discussing our experimental results with internal resistance  $R_1$ , Eq. (6), it

<sup>1</sup> There is a much more advanced Radon–Nikodym technique[10] that can be applied to obtain relaxation rate distribution as matrix spectrum for relaxation type of data such as in Fig. 8. The distribution of the eigenvalues (using the Lebesgue quadrature[11] weight as eigenvalue weight) is an estimator of the distribution of relaxation rates observed in the measurement; Radon–Nikodym approach is much less susceptible to measurement errors compared to inverse Laplace transform type of analysis.

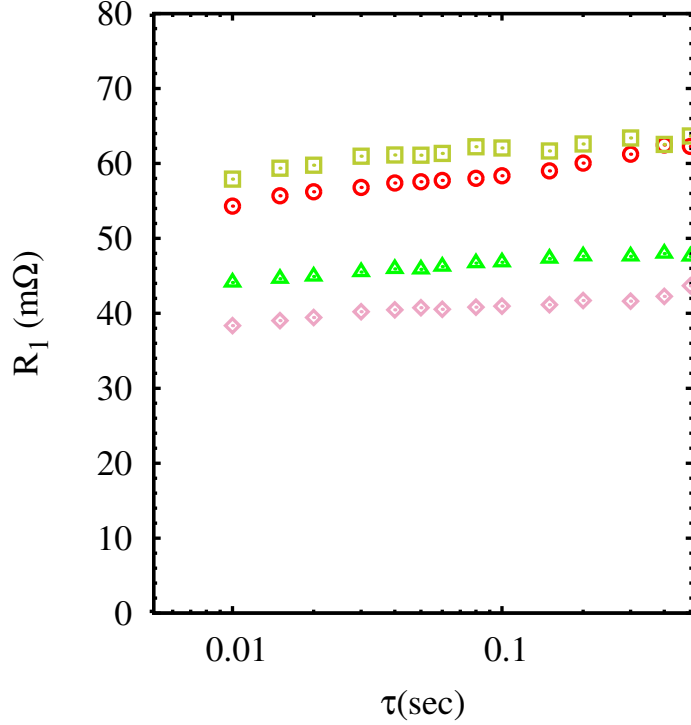
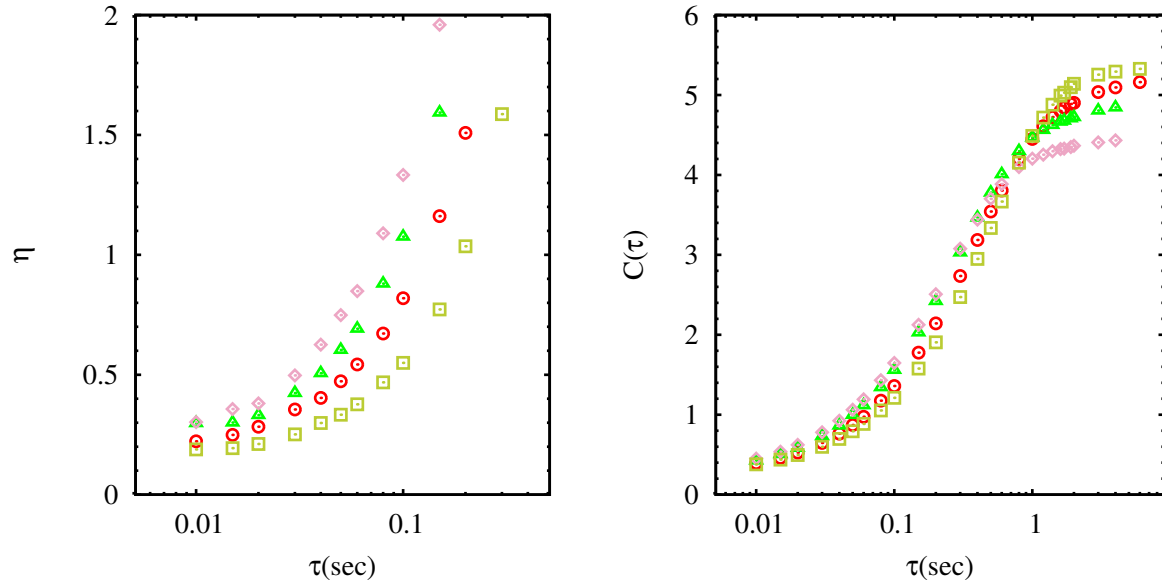


**FIG. 9:** An internal resistance component  $R_1$  from (6) measurement for four commercial supercapacitors AVX-SCCS20B505PRBLE (circles), Eaton-HV1020-2R7505-R (triangles), IC-505DCN2R7Q (squares), and Nesscap-ESHSR-0005C0-002R7 (rhombuses); as a function on  $\tau$ .

is presented in Fig. 9. Measured  $R_1$  does not depend on shorting time at all, the value corresponds to minimal possible internal resistance. Some manufacturers present the internal resistance for different  $\tau$  (e.g. [12] presents internal resistance for 0.01sec and 5sec). In their setup (which assumes constant capacitance and variable resistance) larger  $\tau$  corresponds to current propagation to supercapacitor deep pores, what involves a contribution from  $R_2$ . In our setup we have a constant  $R(\tau) = R_1 = \text{const}$  and instead consider an “effective” capacitance as a function of  $\tau$ , this is how the  $C(\tau)$  is defined in Eq. (7). It has a very clear meaning: the ratio of charge/potential change for the  $\tau$ ; this corresponds to a typical SC setup: discharge as much as you can in a given time  $\tau$ .

In Fig. 10a  $\eta$  as a function of shorting time is presented. Only three potentials  $U_0$ ,  $U_1$ , and  $U_2$  have to be measured; no measurement of exponentially small values is required: the  $U_0 - U_1$  and  $U_2 - U_1$  are not small for actual  $\tau$  values used in the experiment. The potentials  $U_0$ ,  $U_1$ , and asymptotic  $U_2$  are measured directly. The only difficulty that may arise



(a) The dependence of  $\eta$  on shorting time  $\tau$ . (b) The dependence  $C(\tau)$  on shorting time  $\tau$ .

**FIG. 10:** Four commercial 5F, 2.7V supercapacitors: AVX-SCCS20B505PRBLE (circles), Eaton-HV1020-2R7505-R (triangles), IC-505DCN2R7Q (squares), and Nesscap-ESHSR-0005C0-002R7 (rhombuses).

if a supercapacitor has a parasitic discharge: both internal and through  $U(t)$  measurement circuit. A good heuristic for  $U_2$  in case of a substantial self-discharge is the maximal value of  $U(t)$  on inverse relaxation stage. A maximal  $\tau$ , for which a plateau can still be observed, is the value below a characteristic scale of inverse relaxation. For a typical supercapacitor the characteristic scale of inverse relaxation can be estimated as a *multiple* of internal  $R_iC$  (available from Fig. 7 at  $C = 5F$  for the supercapacitors we use). This scale is different from  $R_iC$  (typically several times greater), but about the same order of magnitude.

In Fig. 10b measured  $C(\tau)$  dependence is presented. This is the most informative chart of the inverse relaxation technique. For all four supercapacitors (5F nominal) low  $\tau$  discharge is equivalent to a discharge of  $0.4F$  ideal capacitor. At high  $\tau$  the discharge is equivalent to a  $5F$  nominal capacitor.

### A. Impedance characteristics of the supercapacitors

The biggest advantage of impedance spectroscopy is that it can capture a wide range (many orders) of frequencies<sup>2</sup>. The disadvantages of the technique are: measurement equipment complexity, impedance interpretation difficulty, and typically a low current linear regime, thus non-linear effects are problematic to study[13]. Most manufacturers provide equivalent ESR at fixed frequency  $1000\text{Hz}$  in the datasheets, which is typically several times lower than the one at DC. In this section we apply impedance technique to obtain DC characteristics of supercapacitors. The goal is to compare impedance approach with inverse relaxation.

A common impedance analysis method is Nyquist plot. In Fig. 11 the Nyquist plot  $Z'Z''$  is presented along with ZView fitting by two- $RC$  model for AVX-SCCS20B505PRBLE and Eaton-HV1020-2R7505-R supercapacitors. The impedance measurements have been performed in a frequency range  $10^{-3} \div 10^5\text{Hz}$ . In this range Nyquist plot has a complex behavior caused by a complex internal structure of the device. In supercapacitor applications the frequencies of practical interest are the ones below  $30 \div 50\text{Hz}$ . For simple models (such as in Fig. 1) it would be rather naïve trying to fit many orders of frequency range by a simple circuit of several  $RC$  chains. For these reasons we limit the frequency range by  $10^{-3} \div 30\text{Hz}$ . A simple one- $RC$  model has a vertical asymptotic behavior at low frequencies. Two- $RC$  chains give some slope at low frequencies, observed in Fig. 11. In ZView, a model with two PCE elements (one with small exponent, a second one is close to 1, almost the capacitance) allows to obtain a very good fit of the impedance curve in the entire  $10^{-3} \div 10^5\text{Hz}$  frequency range. The PCE element by itself can be modeled as a sequence of  $RC$  elements[14], thus the value and exponent of PCE describe the supercapacitor's internal structure. However, a limited range of practically interesting frequencies along with interpretation difficulties makes this approach not very appealing.

A very important feature of a supercapacitor, not observed in a regular capacitor, is that the impedance curve depends strongly on DC potential applied. When the DC potential changes from  $0\text{V}$  to  $2.5\text{V}$  the impedance curve shifts to the right (the supercapacitor's

<sup>2</sup> The biggest advantage of impedance spectroscopy is that impedance function is a ratio of two polynomials, thus it can be measured/interpolated/approximated with a high degree of accuracy for the measurements in a wide range (over 9 orders, typically  $10^{-3} \div 10^6\text{Hz}$ ) of frequency responses. However, in time-domain, where exponentially small values need to be measured, a much smaller range of time-scales are accessible (less than 2 orders, often just a single order), hence in standard mathematical techniques, such as inverse Laplace transform, any type of noise/discretization/measurement error/window effect have a huge impact on exponentially small Laplace transform contributions[10]

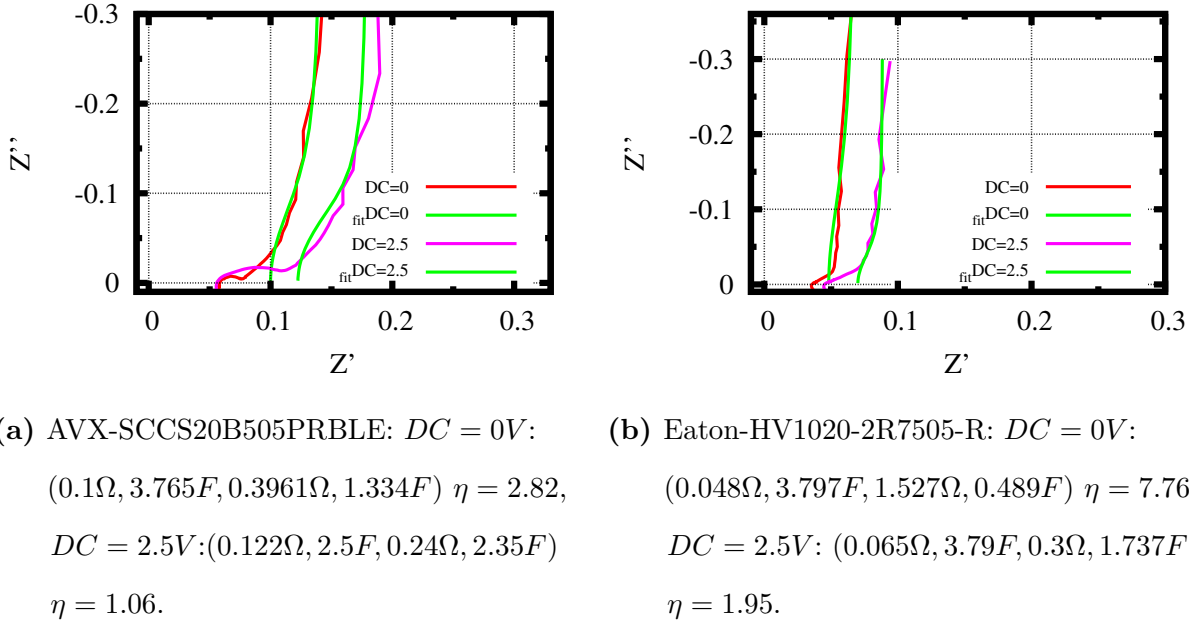


**FIG. 11:** Impedance curves for two commercial supercapacitors with potential offsets  $DC = 0V$  and  $DC = 2.5V$ . The curves are then fitted with two chain  $RC$  model in Fig. 1 using ZView program, the values  $(R_1, C_1, R_2, C_2)$  are obtained from the fitting. Frequency range has been chosen as  $10^{-3} \div 30\text{Hz}$ ; the impedance was measured at very small  $5mV$  AC amplitude.

internal resistance increase) and the Nyquist plot changes substantially. The dependence of the capacitance on the applied potential is a known effect. It can be caused by the density of state changes[15], double layer structure changes[16–19], or redox–active electrolyte processes[20, 21] of both reversible (Faraday’s capacitance) and irreversible (electrochemical decomposition) types.

The data, obtained from  $10^{-3} \div 30\text{Hz}$  impedance fitting differ quite substantially from the results of previous section. While the value of  $R_1$  and total capacitance are similar, the  $\eta$  differ substantially, also it typically decreases with DC potential increase: changes from 2.82 to 1.06 for AVX-SCCS20B505PRBLE and from 7.76 to 1.95 for Eaton-HV1020-2R7505-R, the same behavior was observed in the other supercapacitors we measured.

These measurements make us to conclude that an approach of “stretching” small signal impedance technique down to DC range is not a good idea. The inverse relaxation has important advantages of being close to “natural” fast discharge regime of a supercapacitor

deployment and the measurement technique itself is much simpler than the impedance technique.

#### IV. DISCUSSION

In this work a novel technique for supercapacitors characterization is developed, modeled numerically, and experimentally tested on a number of commercial supercapacitors. The technique does not have any exponentially small value to measure, while, in the same time, all the measurements are performed not in the frequency domain, but in the time domain; the measurement is technically feasible in at least three orders of time-scales. Besides of the simplicity of the technique (no fitting is required), the most important feature of the inverse relaxation approach is its simple automation. Microcontroller-operated two switches and a single ADC can obtain the dependence of an “effective” capacitance on time-scale  $C(\tau)$ , Fig. 10b. The approach can be considered as an alternative to commonly used[12] consideration of a constant capacitance and time-scale dependent internal resistance. Among the advantage of our technique is that it does not require a source of fixed current, what simplify the setup and allows a very high discharge current regime.

Modeling supercapacitors internal structure in electronic circuit software is a common field of study[8, 22–25]. In [26] a voltage rebound effect, shorting and then switching to open circuit was also modeled. However, only in our early work[7] the ratio  $\eta$  of “easy” and “hard” to access capacitance was introduced. Similar pulse-response characteristics of Li-ion batteries have been studied in [27] with an emphasis on time-scale.

The idea to use pulsed load for a battery (primary or secondary) or fuel cell is now widespread. For example GSM standard specifies  $0.575ms$  transmission burst within a  $4.6ms$  period (1/8 duty factor), thus DC-DC chips like [28], that are especially designed for pulsed load, have been used in all modern devices. S.L.Kulakov pioneered an application of pulsed load to metal-air current sources and then, about a decade later, brought out attention to pulsed load technique in [29]. Developed in this paper pulsed technique for supercapacitor characterization is dedicated to his memory.

## Appendix A: Software Modeling

The systems have been modeled in Ngspice circuit simulator. The circuit have been created in gschem program of gEDA project. To run the simulator download[30] the file RCCircuit.zip and decompress it. To test the simulator execute

```
ngspice Farades_y_with_variables.sch.autogen.net.cir
```

Because original gschem+ngspice do not have a convenient parameterisation, a perl script `run_auto.pl` have been developed. To run the simulator with  $\tau = 0.2$ sec execute:

```
perl -w run_auto.pl Farades_y_with_variables.sch 0.2
```

The script takes the `Farades_y_with_variables.sch` which corresponds to three- $RC$  system in Fig. 5 and substitute shorting time  $\tau = 0.2$ . One can modify it accordingly, and run ngspice. The result is saved to `n0_output.txt`.

- [1] Martin Oschatz, Sofiane Boukhalfa, Winfried Nickel, Jan P Hofmann, Cathleen Fischer, Gleb Yushin, and Stefan Kaskel, “Carbide-derived carbon aerogels with tunable pore structure as versatile electrode material in high power supercapacitors,” *Carbon* **113**, 283–291 (2017).
- [2] Adekunle Moshood Abioye and Farid Nasir Ani, “Recent development in the production of activated carbon electrodes from agricultural waste biomass for supercapacitors: a review,” *Renewable and sustainable energy reviews* **52**, 1282–1293 (2015).
- [3] Christian L Mangun, Kelly R Benak, James Economy, and Kenneth L Foster, “Surface chemistry, pore sizes and adsorption properties of activated carbon fibers and precursors treated with ammonia,” *Carbon* **39**, 1809–1820 (2001).
- [4] Arie Borenstein, Ortal Hanna, Ran Attias, Shalom Luski, Thierry Brousse, and Doron Aurbach, “Carbon-based composite materials for supercapacitor electrodes: a review,” *Journal of Materials Chemistry A* **5**, 12653–12672 (2017).
- [5] Aurelien Du Pasquier, Irene Plitz, Serafin Menocal, and Glenn Amatucci, “A comparative study of Li-ion battery, supercapacitor and nonaqueous asymmetric hybrid devices for automotive applications,” *Journal of power sources* **115**, 171–178 (2003).

- [6] Yongju Yoo, Min-Seop Kim, Jong-Kook Kim, Yong Sin Kim, and Woong Kim, “Fast-response supercapacitors with graphitic ordered mesoporous carbons and carbon nanotubes for ac line filtering,” *Journal of Materials Chemistry A* **4**, 5062–5068 (2016).
- [7] ME Kompan and VG Malyshkin, “The Reverse Relaxation Effect and Structure of Porous Electrodes in Supercapacitors,” *Technical Physics Letters* **45**, 45–47 (2019).
- [8] DS Ilyushchenkov, AA Tomasov, and SA Gurevich, “Modeling Charge/Discharge Characteristics of Supercapacitors on the Basis of an Equivalent Scheme with Fixed Parameters,” *Technical Physics Letters* **46**, 80–82 (2020).
- [9] James Larminie, Andrew Dicks, and Maurice S McDonald, *Fuel cell systems explained*, Vol. 2 (J. Wiley Chichester, UK, 2003).
- [10] Aleksandr Vasilievich Bobyl, Andrei Georgievich Zabrodskii, Mikhail Evgenievich Kompan, Vladislav Gennadievich Malyshkin, Olga Valentinovna Novikova, Ekaterina Evgenievna Terukova, and Dmitry Valentinovich Agafonov, “Generalized Radon–Nikodym Spectral Approach. Application to Relaxation Dynamics Study.” ArXiv e-prints (2016), <https://arxiv.org/abs/1611.07386>, arXiv:1611.07386 [math.NA].
- [11] Vladislav Gennadievich Malyshkin, “On Lebesgue Integral Quadrature,” ArXiv e-prints (2018), arXiv:1807.06007 [math.NA].
- [12] Maxwell technologies, (2018), BCAP0005 P270 S01, ESHSR-0005C0-002R7, Document 3001974-EN.3, product list, and Test Procedures for Capacitance, ESR, Leakage Current and Self-Discharge Characterizations of Ultracapacitors.
- [13] ME Kompan, VP Kuznetsov, and VG Malyshkin, “Nonlinear impedance of solid-state energy-storage ionisters,” *Technical Physics* **55**, 692–698 (2010).
- [14] Juraj Valsa and Jiri Vlach, “RC models of a constant phase element,” *International Journal of Circuit Theory and Applications* **41**, 59–67 (2013).
- [15] ME Kompan and VG Malyshkin, “Ultimate capacitance characteristics of graphene electrodes for supercapacitors: Quantum restrictions,” *Technical Physics Letters* **41**, 359–361 (2015).
- [16] Alexei A Kornyshev, “Double-layer in ionic liquids: paradigm change?” (2007).
- [17] Vladimir S Bagotsky, Alexander M Skundin, and Yurij M Volkovich, *Electrochemical power sources: batteries, fuel cells, and supercapacitors* (John Wiley & Sons, 2015).
- [18] Cheng Zhan, Cheng Lian, Yu Zhang, Matthew W Thompson, Yu Xie, Jianzhong Wu, Paul RC Kent, Peter T Cummings, De-en Jiang, and David J Wesolowski, “Computational insights into

materials and interfaces for capacitive energy storage," *Advanced Science* **4**, 1700059 (2017).

[19] Guilherme Volpe Bossa, Rachel Downing, Jacob Abrams, Bjorn K Berntson, and Sylvio May, "Differential Capacitance of Electrolytes at Weakly Curved Electrodes," *The Journal of Physical Chemistry C* **123**, 1127–1135 (2018).

[20] Keren Dai, Xiaofeng Wang, Yajiang Yin, Chenglong Hao, and Zheng You, "Voltage fluctuation in a supercapacitor during a high-g impact," *Scientific reports* **6**, 38794 (2016).

[21] Shuai Ban, Jiujun Zhang, Lei Zhang, Ken Tsay, Datong Song, and Xinfu Zou, "Charging and discharging electrochemical supercapacitors in the presence of both parallel leakage process and electrochemical decomposition of solvent," *Electrochimica Acta* **90**, 542–549 (2013).

[22] Patrik Johansson and Björn Andersson, "Comparison of simulation programs for supercapacitor modelling," Master of Science Thesis. Chalmers University of Technology, Sweden (2008).

[23] Pierre-Olivier Logerais, MA Camara, O Riou, A Djellad, A Omeiri, F Delaleux, and JF Durastanti, "Modeling of a supercapacitor with a multibranch circuit," *international journal of hydrogen energy* **40**, 13725–13736 (2015).

[24] Clarisse Péan, Benjamin Rotenberg, Patrice Simon, and Mathieu Salanne, "Multi-scale modelling of supercapacitors: From molecular simulations to a transmission line model," *Journal of Power Sources* **326**, 680–685 (2016).

[25] Shuang Song, Xiong Zhang, Chen Li, Kai Wang, Xianzhong Sun, Qunhai Huo, Tongzhen Wei, and Yanwei Ma, "Equivalent circuit models and parameter identification methods for lithium-ion capacitors," *Journal of Energy Storage* **24**, 100762 (2019).

[26] Stephen Fletcher, Iain Kirkpatrick, Roderick Dring, Robert Puttock, Rob Thring, and Simon Howroyd, "The modelling of carbon-based supercapacitors: Distributions of time constants and Pascal Equivalent Circuits," *Journal of Power Sources* **345**, 247–253 (2017).

[27] Anup Barai, Kotub Uddin, WD Widanage, Andrew McGordon, and Paul Jennings, "A study of the influence of measurement timescale on internal resistance characterisation methodologies for lithium-ion cells," *Scientific reports* **8**, 21 (2018).

[28] Maxim Integrated, (2019), MAX1687 Step-Up DC-DC Converters with Precise, Adaptive Current Limit for GSM.

[29] MI Danielyan, KS Kulakov, SL Kulakov, VL Tumanov, and ME Kompan, "Increasing the efficiency of metal–air current sources operating in a pulse-train mode," *Technical Physics Letters* **33**, 597–599 (2007).

[30] ME Kompan and VG Malyshkin, (2018), RC simulating program for ngspice. <http://www.ioffe.ru/LNEPS/malyshkin/RCcircuit.zip>.